Lithos 284–285 (2017) 578–587

Contents lists available at ScienceDirect

Lithos

journal homepage: www.elsevier.com/locate/lithos

Compositional zonation of the shallow La Gloria pluton (Central Chile) by late-stage extraction/redistribution of residual melts by channelization: Numerical modeling

A. Aravena [a,b,*], F.J. Gutiérrez [a,c,d], M.A. Parada [a,c], Í. Payacán [a,c], O. Bachmann [e], F. Poblete [a,f]

[a] Departamento de Geología, Facultad de Ciencias Físicas y Matemáticas, Universidad de Chile, Santiago, Chile
[b] Dipartimento di Scienze della Terra, Università di Firenze, Firenze, Italy
[c] Centro de Excelencia de Geotermia de los Andes (CEGA-FONDAP 15090013), Facultad de Ciencias Físicas y Matemáticas, Universidad de Chile, Santiago, Chile
[d] Advanced Mining Technology Center, Facultad de Ciencias Físicas y Matemáticas, Universidad de Chile, Santiago, Chile
[e] Institute of Geochemistry and Petrology, ETH Zurich, Zurich, Switzerland
[f] Géosciences Rennes, Université de Rennes I, Rennes, France

ARTICLE INFO

Article history:
Received 4 January 2017
Accepted 21 May 2017
Available online 28 May 2017

Keywords:
La Gloria pluton
Diking
Zoned pluton
Silicic melt extraction
Rhyolitic magma sources

ABSTRACT

The origin of highly evolved magmas (e.g. rhyolites) has been a long-standing controversy in earth sciences. They are commonly thought to be generated in the upper crust by melt extraction from mush zones, but due to the rapid cooling of magma reservoirs in such shallow and typically cold environments, high magma emplacement rates of intermediate magmas are thought to be necessary to maintain large silicic mushes above the solidus long enough for the high-SiO_2 melts extraction to occur. Late-stage redistribution of interstitial melts (i.e. heat and mass) by channels/dikes within those mushes has been invoked as a mechanism to preserve silicic mushes above their solidi for longer periods (i.e. delaying their final crystallization), but the nature of this process and its implications on plutons zonation are still poorly understood.

Here, using time-dependent numerical modeling, we study the feasibility of late-stage interstitial melt extraction/redistribution by channels/dikes from a crystalline mush. Our model accounts for magma fluid dynamics, extraction of residual melts and thermal evolution of the crystallizing magma system and its hosting rocks, considering the thermal effect of the redistributing material. The model was applied to explain the anatomy of the well-documented La Gloria pluton (LGP, Central Chile), which exhibits increasing contents of SiO_2 and abundant leucocratic dikes toward the margins, interpreted as trapped residual melts generated elsewhere in the magma chamber.

Our results suggest that favorable conditions for extracting late-stage residual melts are reached at temperatures of ~750 °C (60 vol% crystallinity), at least for compositions similar to LGP dikes. Simulations correspond to 30 kyr of reservoir cooling, when the concentric compositional zonation of LGP is reproduced after a short period of extraction (<15 kyr) and outward redistribution of silicic melt, with an extracted mass fraction of up to 0.17. An inward growing crystal-dominated domain is the main source of interstitial melts. A total extracted melt volume of ~7.5 km^3 and a mean extraction rate of ~0.5 km^3/kyr were calculated for LGP conditions. For small magma reservoirs, the extracted rhyolitic melt could reach the upper levels of the magma chamber and the overlying host rock, but it seems unlikely that it can reach the surface to feed large rhyolitic eruptions, at least once recharges have stopped.

1. Introduction

The source of rhyolites has been a controversial topic for decades (Ayalew and Ishiwatari, 2011; Bachmann and Bergantz, 2008; Lee and Morton, 2015; Lundstrom and Glazner, 2016; Mahood and Halliday, 1988; Shellnutt et al., 2012). In recent years, the petrologic community seems to have converged toward two alternatives: (1) rhyolitic melts are formed relatively deep inside the earth (lower/middle crust) and only construct ephemeral magma chambers in the upper crust (Cooper and Kent, 2014; Druitt et al., 2016; Glazner et al., 2015; Gualda et al., 2012); and (2) rhyolites are residual melts extracted "in-situ" from long-lived shallow intermediate magma reservoirs in the upper crust (Bachmann and Bergantz, 2004; Bacon and Druitt, 1988;

Abbreviations: LGP, La Gloria pluton.

* Corresponding author at: Dipartimento di Scienze della Terra, Universitá di Firenze, Via Giorgio La Pira 4, I-50121 Firenze, Italy.
E-mail address: alvaro.aravenaponce@unifi.it (A. Aravena).

http://dx.doi.org/10.1016/j.lithos.2017.05.013
0024-4937/

Deering et al., 2011; Hildreth, 2004). Part of the controversy lies in the fact that several recently published thermal models have concluded that magma emplacement rates required to build and maintain large silicic mushes in the upper crust are too high to allow significant in-situ differentiation in most magmatic systems (Annen, 2009; Annen et al., 2015; Caricchi et al., 2014), although Karakas et al. (2017) have suggested that long-lasting intrusions can modify the thermal budget of the upper crust, reducing the magma emplacement rates required to sustain shallow magma reservoirs.

Intermediate to silicic plutons are one of the main sources of information to understand the origin of silicic magmas on earth, because they should be the solid record left behind by the rhyolitic melts (Bachl et al., 2001; Coint et al., 2013; Gelman et al., 2014; Lee and Morton, 2015; Putirka et al., 2014). Most silicic plutons are geochemically complex ("zoned") as a result of combined processes of magma emplacement, internal differentiation and geochemical interaction with the country rocks. In fact, compositional zonation in plutons has been attributed to a number of processes, including: (1) in-situ fractional crystallization within a crystal-poor convecting magma (Imaoka et al., 2014; Sawka et al., 1990); (2) incomplete mixing/mingling between two or more different magma bodies (Memeti et al., 2010; Zhang et al., 2014); (3) incremental emplacement of different types of magma batches (Hecht et al., 1997); (4) crustal assimilation (Imaoka et al., 2014; Rodríguez et al., 2016); and (5) extraction of high-SiO_2 interstitial melt from a crystalline network, which could generate rhyolitic eruptions (Bachmann and Bergantz, 2004, 2008).

Some mechanisms have been proposed so far to explain the extraction/redistribution of interstitial magmas from crystal mushes: (1) melt extraction following compaction of solid phases (Shirley, 1986), (2) hindered settling and micro-settling (Bachmann and Bergantz, 2004; Lee and Morton, 2015; Miller et al., 1988), (3) gas-filtering (Bachmann and Bergantz, 2006; Sisson and Bacon, 1999), and (4) melt redistribution by a network of channeling dikes (Sleep, 1974; Weinberg, 2006).

Because diking is the main mechanism of felsic magma transport across the upper crust (Petford et al., 1993), leucogranitic dikes are likely testimonies of extraction/redistribution of silicic interstitial melts from a mush. Several previous studies have addressed the nature of granitic magma transport in the crust through dikes, focusing on dikes width (Menand et al., 2015; Petford et al., 1993) and overpressure (Jellinek and DePaolo, 2003). On the other hand, a geochemical approach has been used for studying dike phenomena and the connection between intermediate-felsic plutons, the preserved leucogranite dikes and rhyolites (Glazner et al., 2008; Mills and Coleman, 2013). Gelman et al. (2014), based on simulations that include the maximum melt extraction efficiency at 50–70% crystal volume (Dufek and Bachmann, 2010), obtained a geochemical model to explain the evolution of trace elements in magma reservoirs. However, some applications of the melt extraction model have resulted in inconsistencies between the erupted magma compositions and interstitial melts (Glazner et al., 2008; Streck, 2014). Additionally, a recent study showed the importance of water for increasing the timespan available for exfiltration of silicic liquids (Lee et al., 2015).

In order to determine the feasibility of interstitial melt extraction/redistribution from a highly crystalline reservoir and constrain how this process is registered in the plutonic record, we study the case of La Gloria pluton: a well-studied shallow Andean granitoid pluton, which exhibits increasing values of SiO_2 concentration toward the margins and abundant leucocratic dikes and sills, previously interpreted as trapped residual melts generated elsewhere in the magma chamber (Mahood and Cornejo, 1992). We develop a numerical model that accounts for the main processes that occur within cooling magma reservoirs and tracks the thermal influence of the extraction and redistribution of residual melts by channeling dikes. The model is applied to the study case, producing compositionally and physically consistent results in a timescale compatible with the evolution of shallow reservoirs, thus providing some lights about the thermal effects of the interstitial melt extraction/redistribution. The formulation of our model does not include restrictive assumptions related to this particular pluton, thus it can be potentially applied for explaining the chemical structure (major elements content) of shallow magma reservoirs and the generation of silicic melts in any appropriate study case. Still, it requires the calibration of some input parameters for determining the optimal conditions for the extraction of residual melts, in addition to suitable physical parameters for the studied magma and some geometric constraints.

This paper consists of two main parts: (1) we present a general description of LGP and the reasons which support that it is an appropriate case study for addressing the extraction/redistribution of interstitial melts; and (2) we describe our 2D time-dependent numerical model and we apply it to LGP. We show that the extraction/redistribution of silicic melts is capable of explaining the most remarkable features of LGP (i.e. geochemical zonation, presence of leucocratic dikes, nature of the host rock aureola, among others), and provide some constraints on the volumetric magnitudes, timescales, thermal effects and geochemical consequences that can be involved in processes of interstitial melt extraction/redistribution.

2. Geological outline: La Gloria pluton

La Gloria pluton is a 10 Ma (Deckart et al., 2010) intrusion located 40 km east of Santiago, central Chile (Fig. 1). It shows a N30°W elongated shape and forms part of a mid-Miocene belt of granodiorite and quartz monzonite plutons with similar orientation (Drake et al., 1982). The pluton was emplaced at ~4 km depth into a fold core formed by Oligocene-Miocene continental volcanic and volcanoclastic sequence (Nyström et al., 2003), and shows concentric zonation patterns: quartz monzodiorite and minor granodiorite are observed in the core of the pluton, whereas quartz monzonite and minor granite are recognized along the borders (Cornejo and Mahood, 1997). The pluton exhibits a slight increasing tendency of SiO_2 content toward the margins: the upper zone of LGP shows a mean SiO_2 content of ~65 wt%; whereas the middle level presents a mean concentration of ~63 wt%, reaching minimum values of ~61 wt% (Cornejo, 1990; Cornejo and Mahood, 1997). This zonation pattern is also manifested by slight and regular variations in the concentration of other major elements, such as Al_2O_3 (~17.0 wt% at the core and ~16.3 wt% at the pluton margins), Fe_2O_3 (~5.1 wt% and ~4.5 wt%, respectively), MgO (~2.1 wt% and ~1.6 wt%, respectively) and CaO (~4.2 wt% and ~3.4 wt%, respectively), among others (Cornejo and Mahood, 1997). Mafic minerals also exhibit regular variation trends: LGP margins commonly include amphibole-rich rocks, whereas the pluton core rocks mainly contain biotite and amphibole. Clinopyroxene is locally present at the lower and middle levels of LGP; and Fe—Ti oxides, titanite and apatite are common accessory minerals in the pluton.

Cornejo and Mahood (1997) have shown a roofward increase of fO_2, manifested in higher contents of magnetite toward the margins, likely due to a higher volatile (H_2O, Cl and F) content in the upper parts of the reservoir. Additionally, magnetic susceptibility increases toward LGP margins and roof (Gutierrez et al., 2013), and new experimental data confirm that magnetic susceptibility (K) of LGP is controlled by magnetite crystals, as indicated by K—T experiments results and Curie temperatures in four selected samples (578 ± 2 °C) (Hunt et al., 1995) (Supplementary Fig. 1).

Leucogranite dikes and sills are abundant in LGP and the host rock. They are much more abundant along the uppermost (~50 m) levels of the pluton (Fig. 2a–b) than on the sides of LGP (Fig. 2c). Dikes range from medium-grained biotite + amphibole + titanite granites to fine-grained biotite aplites, while K-feldspar-rich pegmatite dikes are also observed. Dikes show a NNW preferential orientation and exhibit variable widths (centimeters to meters). Most of the narrow dikes, mainly located at the pluton core, are sinuous (Fig. 2d) and locally perturb the mineral fabric of the host rocks, indicating synplutonic emplacement.

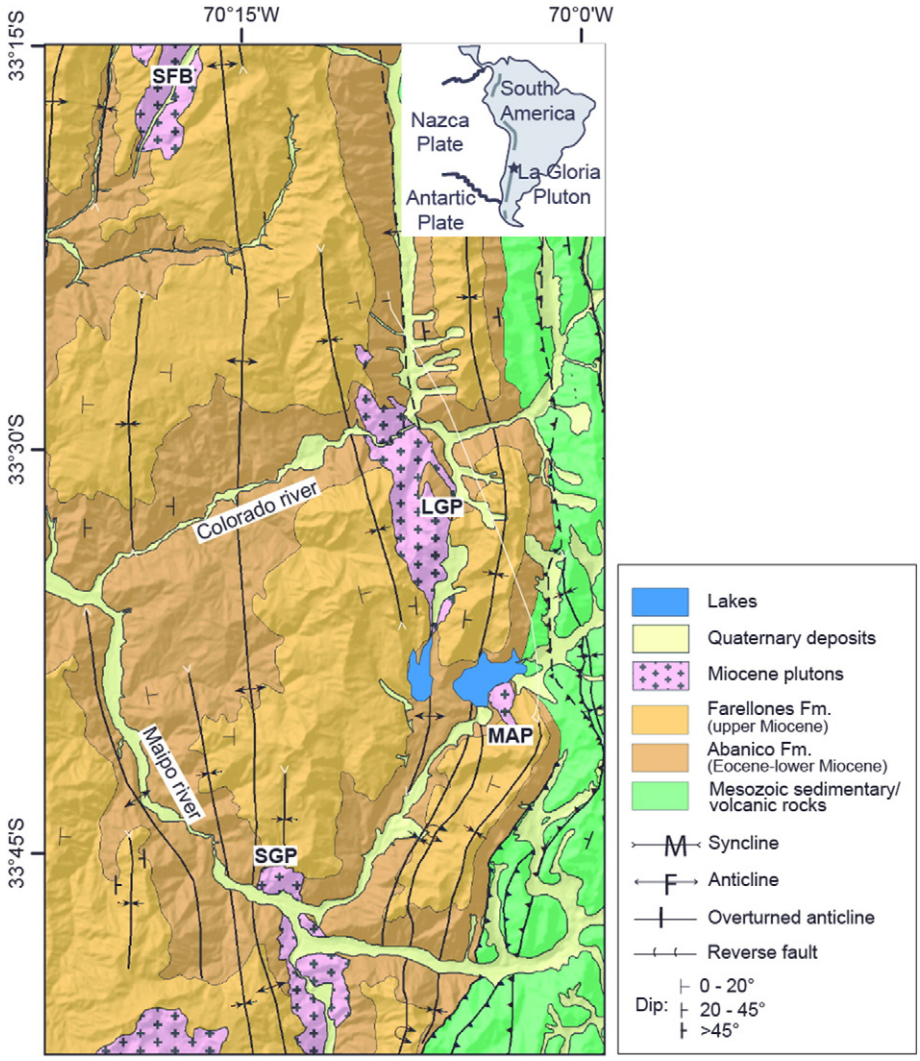

Fig. 1. Geological setting of La Gloria pluton (LGP), Central Chile. Other Miocene intrusive bodies are shown (SFB: San Francisco batholith. MAP: Meson Alto pluton. SGP: San Gabriel pluton).

On the contrary, wider dikes are generally continuous, straight and concentrated at the pluton margins (Fig. 2a–c).

Leucocratic dikes have been interpreted as trapped residual melts generated elsewhere in the magma chamber (Mahood and Cornejo, 1992), thus processes of late-stage melt extraction and upward redistribution by channels are likely to occur in LGP. Because of the absence of textural evidences of mineral compaction, other mechanisms of silicic melts mobilization are expected to be significant in LGP, at least with meaningful consequences on the resulting geochemical composition (particularly, major elements). Given that the host rock exhibits a well-developed contact aureola (particularly, in the upper levels), in addition to the geochemical zonation of the pluton and the pervasive presence of leucocratic dikes, LGP appears as an appropriate case study for addressing the geochemical and thermal effects related to interstitial melt extraction/redistribution by channels from highly crystalline reservoirs, given place to leucogranitic dikes.

3. Time-dependent numerical modeling

In this section, we present a 2D time-dependent model performed by the Finite Element Method by using the software COMSOL Multiphysics, in order to analyze late-stage extraction/redistribution of residual melts from small shallow magma chambers. Our model considers the most relevant processes that cooling magma reservoirs experiment, such as crystallization, heat transfer through the walls/roof and gravity-driven movement of magma (Section 3.1). It also includes a set of equations for modeling the extraction and redistribution of the silicic material, considering the thermal interaction between the redistributing material and the surrounding rocks (Section 3.2). Additionally, although our model does not include restrictive assumptions related to this particular study case and thus it could be potentially applied to any appropriate pluton, a set of input parameters must be calibrated by using data from the specific study case, as described in Section 3.3. Geometric parameters and initial conditions were also derived from the analysis of LGP (see Section 3.3).

3.1. Magma fluid dynamics and thermal evolution

The model considers a system composed by two different domains: (1) magma chamber and (2) host rock. We assume that magma chamber temperature varies with time according to two physical equations. The first equation accounts for the internal heat balance in a crystallizing magma reservoir:

$$\rho_m C_{pm} \frac{\partial T}{\partial t} + \rho_m C_{pm} (\mathbf{u} \cdot \nabla T) = \nabla \cdot (k_m \nabla T) + Q_{Lm} + Q_{er} \quad (1)$$

where ρ_m is the magma density, C_{pm} is the magma heat capacity, T is the

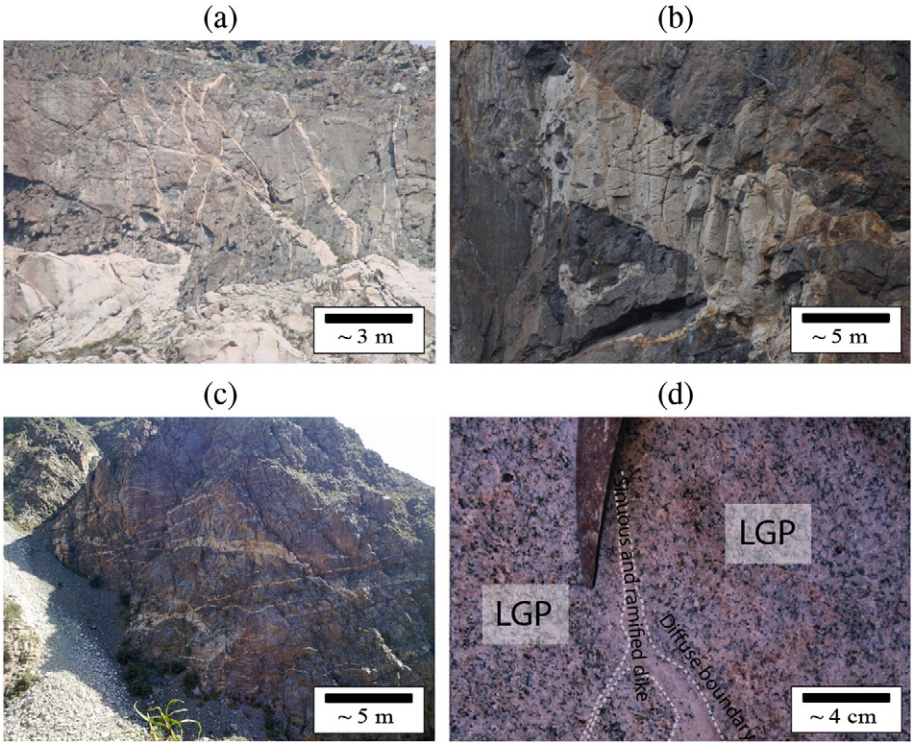

Fig. 2. (a) Leucogranite sills and dikes at the LGP contact with the roof rocks. (b) Leucogranite sill hosted in volcanic rocks of the LGP roof. (c) Narrow leucogranite sills hosted in volcanic strata of the western margin of the pluton. (d) Sinuous and narrow synplutonic dikes emplaced at the core of the LGP.

temperature, t is the time, $\mathbf{u}$ is the magma velocity field, k_m is the magma thermal conductivity, Q_{Lm} is the magma latent heat and Q_{er} is a heat source term related to the extracted/redistributed magma. The second equation accounts for the thermal perturbation derived from host rock-melt interaction:

$$-\mathbf{n}\cdot(k_m\nabla T)=\frac{k_h(\Delta T)}{L_{mh}} \tag{2}$$

where $\mathbf{n}$ is the normal vector to the contact surface, k_h is the host rock thermal conductivity (temperature-dependent expression), L_{mh} is the distance of thermal effect and ΔT is the temperature difference between magma and host rock in the contact.

Furthermore, the magma fluid dynamics is modeled using Eq. (3):

$$\rho_m\left(\frac{\partial\mathbf{u}}{\partial t}+(\mathbf{u}\cdot\nabla)\mathbf{u}\right)=\nabla\cdot\left(\mu_m\left(\nabla\mathbf{u}+\nabla\mathbf{u}^{\mathbf{T}}\right)\right)-\nabla p-\rho_m g \tag{3}$$

where μ_m is the magma dynamic viscosity, p is the magma pressure field and g is the acceleration of gravity.

The thermal regime of the host rock is controlled by Eq. (4):

$$\rho_h C_{ph}\frac{\partial T}{\partial t}=\nabla\cdot(k_h\nabla T)+Q_{er} \tag{4}$$

where ρ_h is the host rock density and C_{ph} is the heat capacity of the host rock (temperature-dependent expression); while Eq. (5) describes the thermal effect derived from the interaction with the magma chamber.

$$\mathbf{n}\cdot(k_h\nabla T)=\frac{k_h(\Delta T)}{L_{mh}} \tag{5}$$

3.2. Residual melt extraction

For modeling the extraction of residual melts, we introduced a variable called 'extraction probability per time unit' (P_E), which is crystallinity-dependant (and thus T-dependant) and is defined as a normal distribution around the 'optimal crystallinity fraction' (crystallinity at which the extraction probability reaches its maximum value) (Gelman et al., 2014), calibrated by using data from the case study (see Section 3.3). The extracted material fraction (i.e. the fraction of silicic melts extracted by channels from highly crystalline zones of the pluton, f_e) is determined by Eq. (6):

$$\frac{\partial f_e}{\partial t}=P_E \tag{6}$$

We obtain the SiO_2 concentration of the extracted/redistributing material (C_{er}) by MELTS as a temperature-dependant variable (Asimow and Ghiorso, 1998; Ghiorso and Sack, 1995), also calibrated using geochemical data from the case study (see Section 3.3). The resulting SiO_2 concentration of the remnant magma (C_{rm}) is calculated by the following expression:

$$C_{rm}=\frac{C_0\cdot((1-f_e)\cdot\rho_{rm}+f_e\cdot\rho_{er})-f_e\cdot\overline{C_{er}}\cdot\rho_{er}}{(1-f_e)\cdot\rho_{rm}} \tag{7}$$

where C_0 is the initial SiO_2 concentration, $\overline{C_{er}}$ is the mean SiO_2 concentration of the extracted/redistributing material, ρ_{rm} is the density of the remnant magma and ρ_{er} is the density of the extracted/redistributing material.

On the other hand, the content of redistributing material by channels (not yet crystallized dikes, f_r) is modeled by Eq. (8), which includes source terms related to the 'extraction probability per time unit', the solidification process of channels (i.e. giving place to leucocratic dikes),

and the effect of the extracted material redistribution as follows:

$$\frac{\partial(f_r)}{\partial t} = (P_E - C_C) - \nabla \cdot \Gamma \tag{8}$$

where C_C represents the melt consumed by crystallization (per time unit) and Γ is the conservative flux of the redistributing material by channels.

We assume that the width of channels follows a gamma distribution ($w_{channels} \sim \Gamma(k_{channels}, \theta_{channels})$, with a mean value of 0.5 m) and the redistributing material velocities are independent of the width of channels. The crystallizing fraction of the redistributing material is obtained using the critical width of channels (i.e. minimum width required for granitic magma ascent without freezing, w_c), defined by the Eq. (9) (Bruce and Huppert, 1989, 1990; Petford et al., 1993):

$$w_c = 1.5 \cdot \left(\frac{S_m}{S_\infty^2}\right) \cdot \left(\frac{\mu_r \kappa_r \alpha}{g \Delta \rho}\right)^{\frac{1}{3}} \tag{9}$$

where μ_r is the redistributing material viscosity, κ_r is the redistributing material thermal diffusivity, α is the ratio between length and width of channels, $\Delta\rho$ is the density difference between redistributing material and host rock, and S_m and S_∞ are Stefan numbers calculated using the following equations:

$$S_m = \frac{L_r}{C_{sr} \cdot (T_{0E} - T_C)} \tag{10}$$

$$S_\infty = \frac{L_r}{C_{sr} \cdot (T_C - T)} \tag{11}$$

where L_r is the solidification latent heat of the redistributing material, C_{sr} is its specific capacity, T_{0E} is the extraction temperature and T_C is the temperature at which magma near the channel walls is immobile and effectively frozen.

The conservative flux of the redistributing material is defined by Eq. (12):

$$\Gamma = \beta \cdot f_r \, (\hat{\mathbf{r}}) \tag{12}$$

where β is a conservative flux proportionality constant and $\hat{\mathbf{r}}$ is the unitary vector of transport direction. As the magma movement is conditioned by the channels solidification criterion, the model is highly insensitive to β for low values of time interval of discretization (Δt). We define the registered differentiated magma content (i.e. leucocratic dikes, f_{ld}) by using the crystallizing fraction of redistributing material (Eq. (13)):

$$\frac{\partial(f_{ld})}{\partial t} = C_C = \frac{f_r \cdot \gamma}{\Delta t} \tag{13}$$

where γ is the rate of crystallizing dikes, dependent on the critical width of channels (see Supplementary Table 1).

For considering the thermal effect of the redistributing melts in the magma chamber and host rock, we include a heat source term according to Eq. (14) (see Eqs. (1) and (4)):

$$Q_{er} = Q_{Lr} + Q_{TIr} \tag{14}$$

where Q_{Lr} is the crystallization latent heat of the redistributing material and Q_{TIr} accounts for the thermal interaction between the redistributing material (i.e. not yet crystallized melt) and the surrounding rocks. Q_{Lr} and Q_{TIr} were obtained by:

$$Q_{Lr} = f_r \cdot \gamma \cdot L_r \cdot \rho_r \tag{15}$$

$$Q_{TIr} = \delta \cdot (1 - \gamma) \cdot \rho \cdot C_p \cdot (T_{0E} - T) \tag{16}$$

where δ is a constant related to the distance of thermal influence, ρ is the external field density (ρ_m or ρ_h) and C_p is the heat capacity of the external field (C_{pm} or C_{ph}). δ is determined by Eq. (17):

$$\delta = \frac{2 \cdot \varepsilon \cdot f_r}{1 - (1 - \gamma) \cdot f_r} \tag{17}$$

where ε is the ratio between the distance of thermal influence and the width of channels, calibrated for obtaining a total heat released from the cooling extracted material (Q_{Te}) as follows:

$$Q_{Te} = V_{Te} \cdot \rho_r \cdot C_p \cdot (T_{0E} - T_{sol}) \tag{18}$$

where V_{Te} is the total volume of extracted material and T_{sol} is the solidus temperature.

3.3. Calibrating the model for the case study

Our model requires the calibration of the following parameters: (1) the fraction of melt that needs to be extracted from the system, (2) the physical conditions for an efficient residual melt extraction and (3) the physical properties of the magma. The mass fraction of extracted melt (f) can be obtained by a mass balance analysis between the leucogranite dikes and the composition of LGP; the physical conditions for a geochemically consistent melt extraction can be obtained by numerical modeling of residual liquids composition according to LGP geochemistry; whereas the physical properties of the magma can be calibrated as temperature-dependent properties by using MELTS and the pluton geochemistry (Asimow and Ghiorso, 1998; Ghiorso and Sack, 1995). It is worth to note that these procedures may be applied to any appropiate case study.

3.3.1. Mass balance

We estimated the fraction of extracted material by a mass balance analysis, using data from the study case. Because of the geochemical zonation of LGP, we consider that the pluton is composed by three geochemical domains: (1) the core composition ($\mathbf{Q_C}$), (2) the margins composition ($\mathbf{Q_M}$) and (3) the dikes composition ($\mathbf{Q_D}$), representing the extracted/redistributed residual melt composition (Table 1). We evaluate the margins composition by a linear combination between core and dikes compositions as follows:

$$\mathbf{Q_M} = f \cdot \mathbf{Q_D} + (1 - f) \cdot \mathbf{Q_C} \tag{19}$$

In order to determine the optimal f value, we minimize the expression E_1 (sum of squared relative errors), indicated in the following equation:

$$E_1(f) = \sum_{i=1}^{N} \left(\frac{Q_{Mi} - f \cdot Q_{Di} - (1 - f) \cdot Q_{Ci}}{Q_{Mi}}\right)^2 \tag{20}$$

Table 1
Whole rock compositions data employed in the mass balance, using $f = 0.17$ (Cornejo and Mahood, 1997).

Oxide	Q_M	Q_C	Q_D	$Q_D \cdot f + Q_C \cdot (1-f)$
SiO_2 [wt%]	65.5 ± 0.9	62.9 ± 0.1	77.5	65,4
TiO_2 [wt%]	0.57 ± 0.01	0.71 ± 0.02	0.15	0,61
Al_2O_3 [wt%]	16.3 ± 0.3	16.95 ± 0.07	13.0	16,28
Fe_2O_3 (t) [wt%]	4.5 ± 0.1	5.1 ± 0.1	0.28	4,3
MnO [wt%]	0.07 ± 0.01	0.07 ± 0.01	0.02	0,06
MgO [wt%]	1.6 ± 0.3	2.1 ± 0.1	0.01	1,7
CaO [wt%]	3.4 ± 0.8	4.2 ± 0.3	1.05	3.7
Na_2O [wt%]	4.2 ± 0.1	4.5 ± 0.2	2.58	4,2
K_2O [wt%]	3.7 ± 0.7	3.2 ± 0.3	5.33	3,6
P_2O_5 [wt%]	0.14 ± 0.01	0.18 ± 0.01	0.02	0,15

where $i = 1, \ldots, N$ represents each oxide (wt%) which satisfies the condition:

$$Q_{Di} > 0.5 \cdot \max(\sigma_{Q_{Mi}}, \sigma_{Q_{Ci}}) \quad (21)$$

where $\sigma_{Q_{Mi}}$ and $\sigma_{Q_{Ci}}$ represent the standard deviations of the oxide i in $\mathbf{Q_M}$ and $\mathbf{Q_C}$, respectively, which was imposed for discarding the effect of measurements with high standard deviations. Mass balance indicates that the melt fraction needed to be extracted from the original composition of LGP is $f = 0.17$ (Table 1 and Fig. 3a).

3.3.2. Optimal conditions for melt extraction

For determining the rheological conditions under which the differentiated melt is efficiently extracted, we model the chemical evolution of a hypothetical cooling magma with an initial composition $\mathbf{Q_M}$, using MELTS (Asimow and Ghiorso, 1998; Ghiorso and Sack, 1995). The best fit for the calculated residual melt composition ($\mathbf{Q_{Dm}}(T)$) is obtained from comparison with the composition of LGP dikes ($\mathbf{Q_D}$), taking into account the optimal temperature calculated for minimizing the expression E_2 (sum of squared relative errors) shown in Eq. (22).

$$E_2(T) = \sum_{i=1}^{N} \left(\frac{Q_{Di} - Q_{Dmi}(T)}{Q_{Di}} \right)^2 \quad (22)$$

where $i = 1, \ldots, N$ represents each oxide (wt%) which satisfies the condition presented in the Eq. (21).

Optimal physical conditions were reached when $T = 750 \pm 10$ °C (crystallinities of ~60 vol%; Fig. 3b). It is important to note that these conditions are consistent with the 'extraction crystallinity window' defined by Dufek and Bachmann (2010), and the results presented by Gelman et al. (2014).

3.3.3. Geometry, initial conditions and physical parameters

Based on geological considerations of LGP (Cornejo and Mahood, 1997), simulations consider the evolution of a shallow reservoir (4.0 km depth) with a section of ~4 km wide and ~3 km height and initial SiO_2 content and temperature of 65 wt% and 900 °C, respectively. On the other hand, the initial host rock temperature was imposed using a geothermal gradient of 30 °C/km. Because we assume a moderate value of initial temperature and the absence of external heat sources, simulations only describe the last stage of the magma chamber cooling history, making the simulated time shorter than the expected emplacement timespan of shallow felsic plutons (Memeti et al., 2010; Schoene et al., 2012). The total simulation time is 30 kyr, timespan during which the whole system crystallizes.

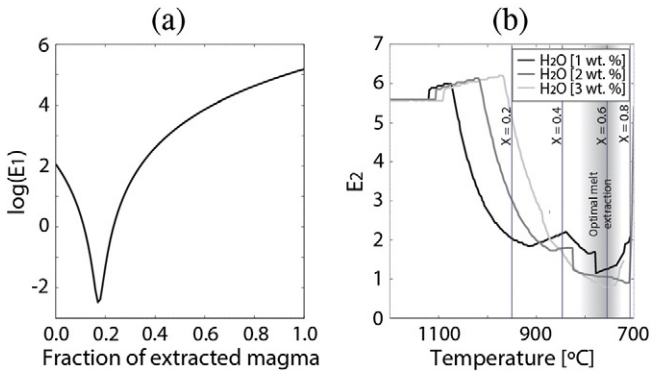

Fig. 3. (a) Logarithm of the sum of squared relative errors (E_1) derived from the mass balance model, versus the fraction of extracted magma. (b) Sum of squared relative errors (E_2) derived from the comparison between leucocratic dikes composition and numerically-simulated composition, versus simulated temperature. Modeled crystallinity (X) and the range of optimal melt extraction (Dufek and Bachmann, 2010) are also included.

Because LGP was emplaced in the core of an anticline fold (Gutierrez et al., 2013; Payacán et al., 2014), we imposed a radial channels propagation from the magma reservoir, following the fractures usually observed around fold axial planes.

A summary of the variable denominations is presented in Table 2, whereas the input parameters employed on numerical simulations and the expressions used for calculating the physical parameters are listed in supplementary Table 1. In particular, the temperature-dependent parameters were mainly obtained from thermodynamic simulations by MELTS (Asimow and Ghiorso, 1998; Ghiorso and Sack, 1995) (Fig. 4).

3.4. Results

The LGP compositional evolution is considered a continuous process that occurs in contiguous and changing zones: core and rim domains. To illustrate the differences between them, Fig. 5 shows some results after 1 and 10 kyr of reservoir evolution. Temperature and velocity fields of the core indicate a highly convective and weakly thermally isolated core after 1 kyr cooling; whereas a substantially less convective, smaller and more thermally isolated core domain is developed after 10 kyr

Table 2
Summary of variable denominations.

Symbol [Units]	Name
ρ_m [kg/m^3]	Magma density
C_{pm} [J/(K·kg)]	Magma heat capacity
T [°C]	Temperature
t [s]	Time
$\mathbf{u}$ [m/s]	Magma chamber velocity field
k_m [W/(K·m)]	Magma thermal conductivity
Q_{Lm} [W/m^3]	Magma latent heat
Q_{er} [W/m^3]	Heat source related to the extracted/redistributed material
k_h [W/(K·m)]	Host rock thermal conductivity
L_{mh} [m]	Distance of thermal effect
μ_m [Pa·s]	Magma dynamic viscosity
p [Pa]	Magma pressure field
g [m/s^2]	Gravity acceleration
ρ_h [kg/m^3]	Host rock density
C_{ph} [J/(K·kg)]	Host rock heat capacity
P_E [1/s]	Extraction probability per time unit
f_e [−]	Extracted material fraction
C_{er} [wt.%]	Extracted/redistributing material SiO_2 concentration
C_{rm} [wt.%]	Remnant magma SiO_2 concentration
C_0 [wt.%]	Initial SiO_2 concentration
ρ_{rm} [kg/m^3]	Remnant magma density
ρ_{er} [kg/m^3]	Extracted/redistributing material density
f_r [−]	Redistributing material fraction
C_C [1/s]	Channels' melt consumed by crystallization per time unit
Γ [m/s]	Conservative flux of redistributing material
$w_{channels}$ [m]	Width of channels
w_c [m]	Critical width of channels
μ_r [Pa·s]	Redistributing material dynamic viscosity
κ_r [m^2/s]	Redistributing material thermal diffusivity
α [−]	Length-width rate of channels
S_m [−]	Stefan number
S_∞ [−]	Stefan number
L_r [J/kg]	Latent heat of solidification of the redistributing material
C_{sr} [J/(K·kg)]	Specific capacity of the redistributing material
T_{0E} [°C]	Initial extracted material temperature
T_C [°C]	Temperature at which magma near the channel walls is effectively frozen
β [m/s]	Conservative flux proportionality constant
f_{ld} [−]	Registered leucocratic dikes fraction
γ [−]	Rate of crystallization of redistributing material
Q_{Lr} [W/m^3]	Latent heat of redistributing material crystallization
Q_{Trr} [W/m^3]	Heat source related to the thermal interaction between redistributing material and surrounding rocks
δ [−]	Constant related to the distance of thermal influence
ε [−]	Ratio between the distance of thermal influence and the channel width
Q_{Te} [J]	Total heat released from the cooling extracted material
V_{Te} [m^3]	Total volume of extracted material

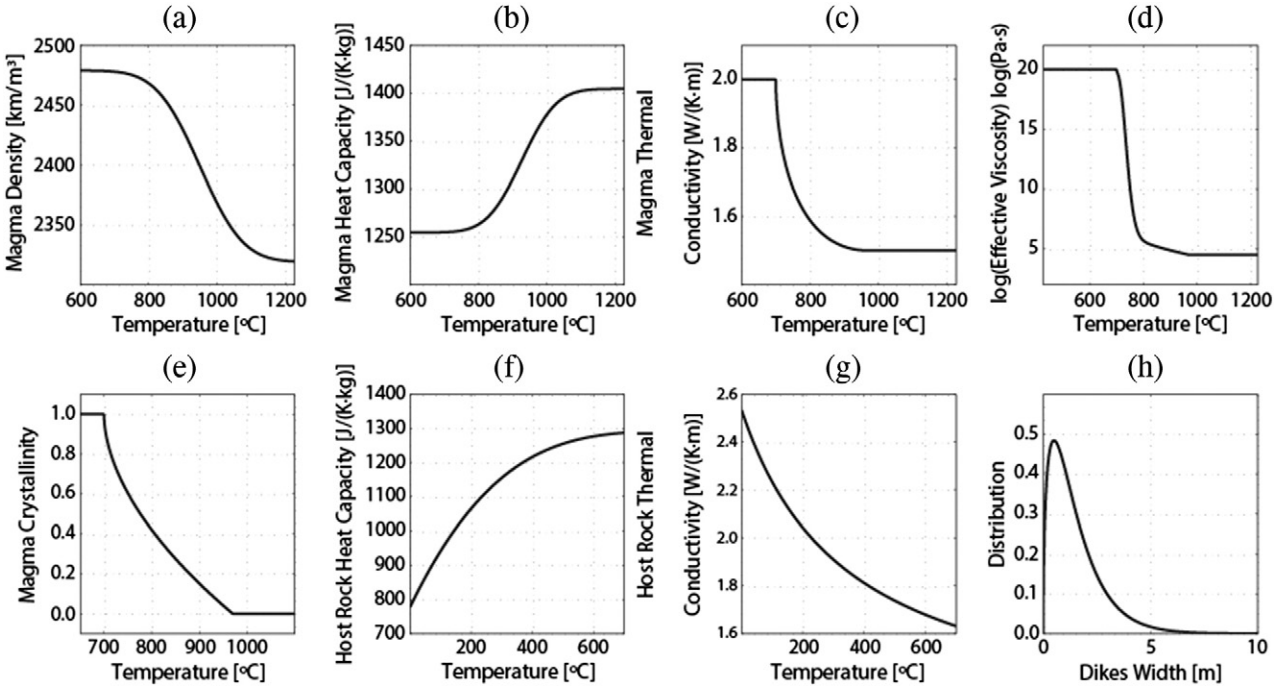

Fig. 4. Temperature-dependence of parameters and physical properties used in our model. (a) Magma density. (b) Magma heat capacity. (c) Magma thermal conductivity. (d) Logarithm of the effective viscosity. (e) Crystallinity. (f) Host rock heat capacity. (g) Host rock thermal conductivity. (h) Distribution of dikes width.

cooling, as a consequence of an inward growth of the highly crystalline rim domain. At the end of the simulation (i.e. 30 kyr), the compositional zonation of LGP is reproduced (Fig. 6a) and the distribution of felsic dikes is clearly concentrated in the upper levels of LGP and roof rocks (Fig. 6b), as it is observed in the field (see Fig. 2a–c for comparison).

The temporal evolution of some relevant parameters is shown in Fig. 7, where we compare results obtained in representative spots of the core and rim domains. The melt extraction is a short-lasting (<15 kyr) process compared with the total emplacement period, and a maximum mass fraction of extracted melt of about 0.17 was obtained at the core domain (Fig. 7a), which is substantially higher than the <0.05 calculated for the rim domain.

Because the core cools slower than the rim domain (Fig. 7c), crystallization proceeds inward, giving rise to a crystal-dominated external zone (Figs. 5b and 7d). This implies that the conditions for an efficient melt extraction survive shorter timespans toward the pluton rim (Fig. 7b). Consequently, the amount of trapped interstitial melts is progressively higher toward the margins (particularly roofward), giving rise to an upper zone characterized by high concentrations of felsic dikes (Fig. 7b). This difference in the resulting concentration of felsic dikes is also yielded because the convective magma core is the main source of silicic melts, which feed the roof zones during the whole magma reservoir cooling history, whereas the lateral zones are feeding leucogranite melts only during the early stages of the magma reservoir cooling. Because of trapped interstitial melts are volatile saturated, we expect that oxidation conditions also increase roofward, allowing crystallization of large amount of magnetite, as shown by Cornejo and Mahood (1997) and is confirmed by new magnetic data.

Simulations indicate that the upward redistribution of felsic melts (Fig. 6b) generates a thermal perturbation of the host rocks resulting in a thermal aureole with maximum temperatures at the pluton contact slightly higher than 500 °C (Fig. 8a), substantially less than the solidus temperature. Thus, the cooling rate of the transported melts out of the pluton should abruptly increase, leading to melt solidification near the magma chamber limits. At a given distance to the contact, temperatures are higher at the roof rocks and survive longer times than at wall rocks (Fig. 8b), allowing longer periods of felsic melt redistribution before complete channels crystallization is reached (i.e. giving place to the observed leucocratic dikes). On the contrary, lower temperatures are observed outward from the pluton contact within the lower host rocks (Fig. 8b), which imply that the crystallization rates of silicic melts injected at these levels were higher, hindering channels propagation.

4. Discussion and concluding remarks

We developed a numerical model for studying the feasibility and implications (i.e. mass and heat redistribution, geochemical zonation) of interstitial melt extraction/redistribution from a crystalline reservoir,

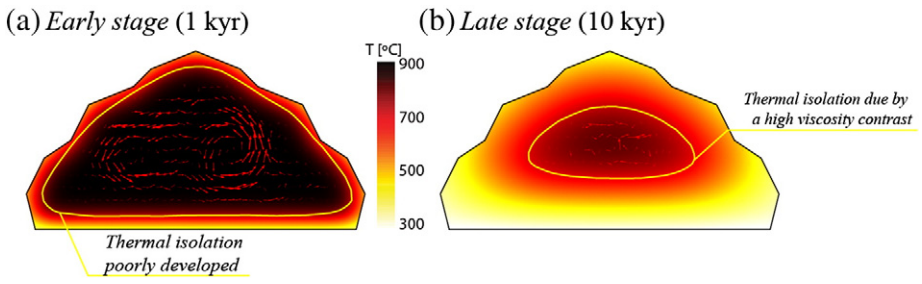

Fig. 5. Simulated temperature and velocity fields (arrows) shown in a representative cross section of LGP chamber after 1 and 10 kyr magma cooling, respectively. The limit between the core and crystal-rich rim domain corresponds to a thermal isolation boundary (yellow curve), which propagates inward with time.

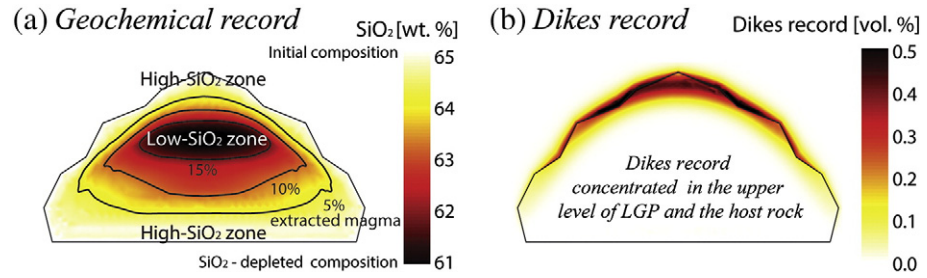

Fig. 6. (a) SiO_2 content distribution and fraction of extracted leucocratic material (black contours), obtained after 30 kyr simulation, shown in a representative cross section of LGP. (b) Abundance and distribution of dikes within the pluton and host rocks, obtained after 30 kyr simulation (shown in the same cross section).

and we applied it to a well-documented, appropriate case study (La Gloria pluton, Central Andes). The model was able to reproduce the general compositional characteristics of the pluton, the distribution of leucocratic dikes and the thermal aureola observed in the host rocks, providing some quantitative constraints for understanding the volumes, space scales and timescales involved in processes of interstitial melt extraction/redistribution.

Results indicate that a highly crystalline rim zone grows at the edge of the reservoir, serving as a thermal insulator for the convective core and thus controlling the crystallization history of the pluton and the extraction dynamics of residual melts. The upward extraction of late-stage interstitial melts from the inward growing rim domain leads to a geochemically zoned magma chamber, with a SiO_2-depleted core, and a SiO_2-enriched ceiling, thus reproducing the geochemical zonation of LGP. Furthermore, the optimal conditions of residual melt extraction (i.e. T = 750 °C and X = 0.6) are consistent with the presence of a crystalline mush and with the 'extraction crystallinity window' defined by Dufek and Bachmann (2010).

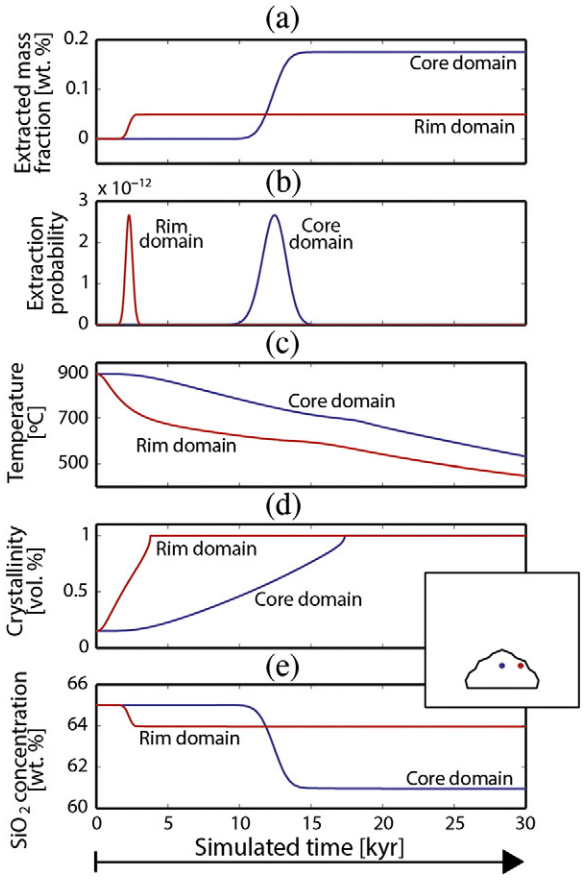

Fig. 7. Relevant parameter variations with time obtained during 30 kyr simulation, using the results obtained at representative spots of core and rim domains. Note that, at the interval 10–15 kyr, the core spot experimented the maximum extracted mass fraction together with the optimal extraction probability, giving rise to a SiO_2 depletion. Similar variations were also obtained at the rim spot, but substantially less intense and at an earlier stage.

For the input conditions that we chose, the total volume of extracted materials (solidified dikes and migrating melts) reached its maximum value after ~15 kyr simulation; afterward the volume of preserved melts decreases as solidification of channels continues (i.e. giving place to leucocratic dikes) up to 30 kyr cooling. The total calculated volume of extracted melts (~7.5 km^3) is twice the volume of the computed dikes into the country rocks (Fig. 9). This total melt volume was extracted during 15 kyr, giving rise to a mean melt extraction rate of about 0.5 km^3/kyr, which is one magnitude order lower than the estimated minimum melt injection rate to prevent its freezing in the upper crust (Gelman et al., 2013; Menand et al., 2015). However, if one considers that a maximum volume of extracted melts (~4 km^3) was obtained at about 15 kyr during a short timespan (≤ 5 kyr, Fig. 9b), a melt extraction rate of ≥0.8 km^3/kyr can be obtained.

While the calculated volume of extracted melt is large enough to have led to volcanic eruptions, their water-saturated, near-eutectic granitic composition can lead to fast crystallization due to ascent-derived decompression and thermal interaction with the country rocks, hindering upward channels propagation to reach the surface and/or construct shallower magma reservoirs capable of preserving whole scale convection. In this scenario, the extracted liquids are mainly concentrated in the upper levels of the pluton and at the contact with the roof rocks, which reasonably match with the observed dikes and sills distribution in LGP. Accordingly, for small magma reservoirs such as LGP, it seems unlikely that the extracted melt can reach the surface and feed rhyolitic eruptions, at least for the conditions and input parameters here chosen (i.e. aspect-ratio of the pluton, absence of magma recharge).

Melt extraction efficiency in a given magmatic system depends on the different timespans during which the extraction operates: the higher the cooling rate is, the lower the melt extraction efficiency should be. Consequently, we suggest that larger magma reservoirs with low aspect ratio (slowing down cooling; Gutiérrez and Parada (2010)) and silicic composition (efficient latent heat buffering; Huber et al. (2009), Sliwinski et al. (2015)) are required to produce efficient and sustained extraction of silicic melts, which could feed volcanic eruptions and/or participate in ore-forming processes. For example, in order to sustain an ignimbrite eruption of 100 km^3 (e.g. Pudahuel ignimbrite, 135–170 km^3 DRE) (Wall et al., 2001), a magma reservoir of 10,000–20,000 km^3 is required (two orders of magnitude larger than LGP), if the highest magma extraction rate calculated for LGP is maintained. For larger eruptions (e.g., Carpenter Ridge Tuff) (Bachmann et al., 2014), even larger reservoirs, or higher extraction rates, would be necessary, requiring deeper magma source, favorable structural settings

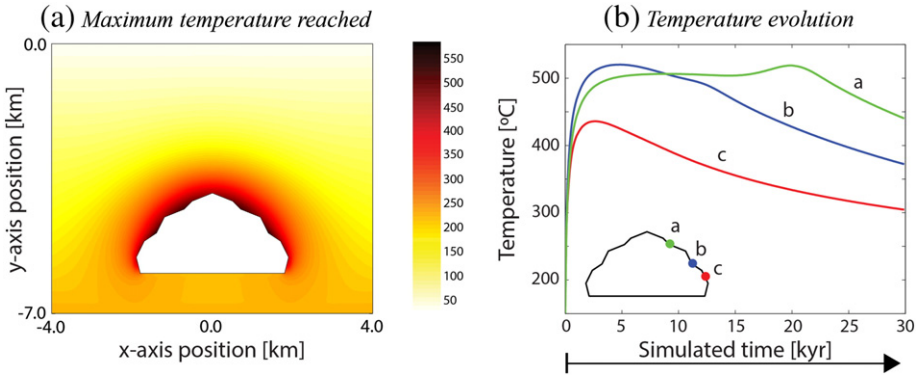

Fig. 8. (a) LGP cross sections showing the maximum temperatures of the host rock aureola (reached at different moments). (b) Temperature variations with simulation times obtained at selected sites of the aureola, located at 30 m out of LGP. Temperatures are higher roofward, favoring dike propagation into the host rock.

and/or vigourous magma recharge. Hence, the numerous shallow Miocene plutons of central Chile would not capable of feeding individually ignimbrite-forming eruptions. However, they form part of a complex and probably interconnected intrusive belt that also contains large, batholithic bodies (Fig. 1). This intrusive belt is related to large-scale ore formation processes and, according to our results, could potentially feed ignimbrite-forming eruptions by late extraction/redistribution of silicic magmas, potentially requiring the aggregation of several pockets of melt formed in different areas of a long-lived upper crustal mush zone. In this sense, small plutons represent ideal study cases for analyzing these processes at a local scale, and the connection between them could be the key for understanding the regional consequences related to timespans characterized by intense plutonic activity, and its relation with rhyolitic volcanism.

Supplementary data to this article can be found online at http://dx.doi.org/10.1016/j.lithos.2017.05.013.

Funding and acknowledgments

This research has been funded by the FONDECYT 11100241, REDES 150063 and PBCT-PDA07 projects granted by CONICYT. A. Aravena was supported by the grant CONICYT N°72160016. I. Payacán was supported by the grant CONICYT N°21151102.

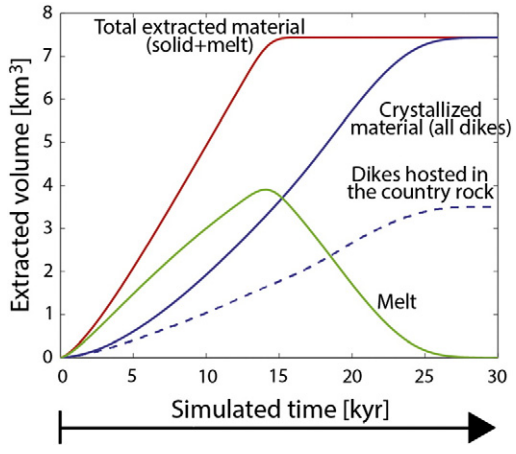

Fig. 9. Variations of volume of extracted/redistributed melts by dikes, with simulation time. Red curve represents the redistributed melt volume (as solidified and flowing dike volumes) accumulated at any moment of the 30 kyr simulation. Green curve represents the volume of preserved melt during diking transportation at any moment of the 30 kyr simulation. Blue curves indicate the accumulated volume of dikes at any moment of the 30 kyr simulation. Clearly, the total extracted material is the sum of crystallized material and melt.

References

Annen, C., 2009. From plutons to magma chambers: thermal constraints on the accumulation of eruptible silicic magma in the upper crust. Earth and Planetary Science Letters 284 (3), 409–416.
Annen, C., Blundy, J.D., Leuthold, J., Sparks, R.S.J., 2015. Construction and evolution of igneous bodies: towards an integrated perspective of crustal magmatism. Lithos 230, 206–221.
Asimow, P.D., Ghiorso, M.S., 1998. Algorithmic modifications extending MELTS to calculate subsolidus phase relations. American Mineralogist 83, 1127–1132.
Ayalew, D., Ishiwatari, A., 2011. Comparison of rhyolites from continental rift, continental arc and oceanic island arc: implication for the mechanism of silicic magma generation. Island Arc 20 (1), 78–93.
Bachl, C.A., Miller, C.F., Miller, J.S., Faulds, J.E., 2001. Construction of a pluton: evidence from an exposed cross section of the searchlight pluton, Eldorado Mountains, Nevada. Geological Society of America Bulletin 113 (9), 1213–1228.
Bachmann, O., Bergantz, G., 2004. On the origin of crystal-poor rhyolites: extracted from batholithic crystal mushes. Journal of Petrology 45 (8), 1565–1582.
Bachmann, O., Bergantz, G.W., 2006. Gas percolation in upper-crustal silicic crystal mushes as a mechanism for upward heat advection and rejuvenation of near-solidus magma bodies. Journal of Volcanology and Geothermal Research 149 (1), 85–102.
Bachmann, O., Bergantz, G., 2008. Rhyolites and their source mushes across tectonic settings. Journal of Petrology 49 (12), 2277–2285.
Bachmann, O., Deering, C.D., Lipman, P.W., Plummer, C., 2014. Building zoned ignimbrites by recycling silicic cumulates: insight from the 1000 km^3 Carpenter Ridge Tuff, CO. Contributions to Mineralogy and Petrology 167 (6), 1–13.
Bacon, C.R., Druitt, T.H., 1988. Compositional evolution of the zoned calcalkaline magma chamber of Mount Mazama, Crater Lake, Oregon. Contributions to Mineralogy and Petrology 98 (2), 224–256.
Bruce, P.M., Huppert, H.E., 1989. Thermal control of basaltic fissure eruptions. Nature 342 (6250), 665–667.
Bruce, P.M., Huppert, H.E., 1990. Solidification and Melting Along Dykes by the Laminar Flow of Basaltic Magma, Magma Transport and Storage. pp. 87–101.
Caricchi, L., Simpson, G., Schaltegger, U., 2014. Zircons reveal magma fluxes in the Earth/'s crust. Nature 511 (7510), 457–461.
Clauser, C., Huenges, E., 1995. Thermal Conductivity of Rocks and Minerals, Rock Physics & Phase Relations: A Handbook of Physical Constants. pp. 105–126.
Coint, N., Barnes, C., Yoshinobu, A., Chamberlain, K., Barnes, M., 2013. Batch-wise assembly and zoning of a tilted calc-alkaline batholith: field relations, timing, and compositional variation. Geosphere 9 (6), 1729–1746.
Cooper, K.M., Kent, A.J., 2014. Rapid remobilization of magmatic crystals kept in cold storage. Nature 506 (7489), 480–483.
Cornejo, P.C., 1990. Geology, Mineral Compositions, and Magmatic Gradients of a Zoned Pluton: La Gloria Pluton, Central Chilean Andes. (Msc. Thesis). Stanford University (160 pp.).
Cornejo, P.C., Mahood, G.A., 1997. Seeing past the effects of re-equilibration to reconstruct magmatic gradients in plutons: La Gloria Pluton, central Chilean Andes. Contributions to Mineralogy and Petrology 127 (1–2), 159–175.
Deckart, K., Godoy, E., Bertens, A., Jerez, D., Saeed, A., 2010. Barren Miocene granitoids in the Central Andean metallogenic belt, Chile: geochemistry and Nd-Hf and U-Pb isotope systematics. Andean Geology 37 (1), 1–31.
Deering, C., Bachmann, O., Vogel, T., 2011. The Ammonia Tanks Tuff: erupting a melt-rich rhyolite cap and its remobilized crystal cumulate. Earth and Planetary Science Letters 310 (3), 518–525.
Drake, R., Vergara, M., Munizaga, F., Vicente, J., 1982. Geochronology of Mesozoic-Cenozoic magmatism in central Chile, lat. 31–36 S. Earth-Science Reviews 18 (3), 353–363.

Druitt, T., Mercier, M., Florentin, L., Deloule, E., Cluzel, N., Flaherty, T., Médard, E., Cadoux, A., 2016. Magma storage and extraction associated with plinian and interplinian activity at Santorini caldera (Greece). Journal of Petrology 57 (3), 461–494.
Dufek, J., Bachmann, O., 2010. Quantum magmatism: magmatic compositional gaps generated by melt-crystal dynamics. Geology 38 (8), 687–690.
Gelman, S.E., Gutiérrez, F.J., Bachmann, O., 2013. On the longevity of large upper crustal silicic magma reservoirs. Geology 41 (7), 759–762.
Gelman, S.E., Deering, C.D., Bachmann, O., Huber, C., Gutiérrez, F.J., 2014. Identifying the crystal graveyards remaining after large silicic eruptions. Earth and Planetary Science Letters 403, 299–306.
Ghiorso, M.S., Sack, R.O., 1995. Chemical mass transfer in magmatic processes IV. A revised and internally consistent thermodynamic model for the interpolation and extrapolation of liquid-solid equilibria in magmatic systems at elevated temperatures and pressures. Contributions to Mineralogy and Petrology 119 (2–3), 197–212.
Glazner, A.F., Coleman, D.S., Bartley, J.M., 2008. The tenuous connection between high-silica rhyolites and granodiorite plutons. Geology 36 (2), 183–186.
Glazner, A.F., Coleman, D.S., Mills, R.D., 2015. The Volcanic-Plutonic Connection.
Gualda, G.A., Pamukcu, A.S., Ghiorso, M.S., Anderson Jr., A.T., Sutton, S.R., Rivers, M.L., 2012. Timescales of quartz crystallization and the longevity of the Bishop giant magma body. PloS One 7 (5), e37492.
Gutiérrez, F., Parada, M.A., 2010. Numerical modeling of time-dependent fluid dynamics and differentiation of a shallow basaltic magma chamber. Journal of Petrology 51 (3), 731–762.
Gutierrez, F., Payacán, I., Gelman, S., Bachmann, O., Parada, M., 2013. Late-stage magma flow in a shallow felsic reservoir: merging the anisotropy of magnetic susceptibility record with numerical simulations in La Gloria Pluton, central Chile. Journal of Geophysical Research - Solid Earth 118 (5), 1984–1998.
Hecht, L., Vigneresse, J., Morteani, G., 1997. Constraints on the origin of zonation of the granite complexes in the Fichtelgebirge (Germany and Czech Republic): evidence from a gravity and geochemical study. Geologische Rundschau 86 (1), S93–S109.
Hildreth, W., 2004. Volcanological perspectives on Long Valley, Mammoth Mountain, and Mono Craters: several contiguous but discrete systems. Journal of Volcanology and Geothermal Research 136 (3), 169–198.
Huber, C., Bachmann, O., Manga, M., 2009. Homogenization processes in silicic magma chambers by stirring and mushification (latent heat buffering). Earth and Planetary Science Letters 283 (1), 38–47.
Hunt, C.P., Moskowitz, B.M., Banerjee, S.K., 1995. Magnetic Properties of Rocks and Minerals, Rock Physics & Phase Relations: A Handbook of Physical Constants. pp. 189–204.
Imaoka, T., Nakashima, K., Kamei, A., Hayasaka, Y., Ogita, Y., Ikawa, T., Itaya, T., Takahashi, Y., Kagami, H., 2014. Anatomy of the Cretaceous Hobenzan pluton, SW Japan: internal structure of a small zoned pluton, and its genesis. Lithos 208, 81–103.
Jellinek, A.M., DePaolo, D.J., 2003. A model for the origin of large silicic magma chambers: precursors of caldera-forming eruptions. Bulletin of Volcanology 65 (5), 363–381.
Karakas, O., Degruyter, W., Bachmann, O., Dufek, J., 2017. Lifestime and size of shallow magma bodies controlled by crustal-scale magmatism. Nature Geoscience.
Lee, C.-T.A., Morton, D.M., 2015. High silica granites: terminal porosity and crystal settling in shallow magma chambers. Earth and Planetary Science Letters 409, 23–31.
Lee, C.-T.A., Morton, D.M., Farner, M.J., Moitra, P., 2015. Field and model constraints on silicic melt segregation by compaction/hindered settling: the role of water and its effect on latent heat release. American Mineralogist 100 (8–9), 1762–1777.
Lundstrom, C.C., Glazner, A.F., 2016. Silicic magmatism and the volcanic–plutonic connection. Elements 12 (2), 91–96.
Mahood, G.A., Cornejo, P.C., 1992. Evidence for ascent of differentiated liquids in a silicic magma chamber found in a granitic pluton. Transactions of the Royal Society of Edinburgh: Earth Sciences 83 (1–2), 63–69.
Mahood, G.A., Halliday, A.N., 1988. Generation of high-silica rhyolite: a Nd, Sr, and O isotopic study of Sierra La Primavera, Mexican Neovolcanic Belt. Contributions to Mineralogy and Petrology 100 (2), 183–191.
Memeti, V., Paterson, S., Matzel, J., Mundil, R., Okaya, D., 2010. Magmatic lobes as "snapshots" of magma chamber growth and evolution in large, composite batholiths: an example from the Tuolumne intrusion, Sierra Nevada, California. Geological Society of America Bulletin 122 (11–12), 1912–1931.
Menand, T., Annen, C., Saint Blanquat, M., 2015. Rates of magma transfer in the crust: insights into magma reservoir recharge and pluton growth. Geology 43 (3), 199–202.
Miller, C.F., Watson, E.B., Harrison, T.M., 1988. Perspectives on the source, segregation and transport of granitoid magmas. Transactions of the Royal Society of Edinburgh: Earth Sciences 79 (2–3), 135–156.
Mills, R.D., Coleman, D.S., 2013. Temporal and chemical connections between plutons and ignimbrites from the Mount Princeton magmatic center. Contributions to Mineralogy and Petrology 165 (5), 961–980.
Nyström, J.O., Vergara, M., Morata, D., Levi, B., 2003. Tertiary volcanism during extension in the Andean foothills of central Chile (33 15′–33 45′ S). Geological Society of America Bulletin 115 (12), 1523–1537.
Payacán, I., Gutiérrez, F., Gelman, S.E., Bachmann, O., Parada, M.Á., 2014. Comparing magnetic and magmatic fabrics to constrain the magma flow record in La Gloria pluton, central Chile. Journal of Structural Geology 69, 32–46.
Petford, N., Kerr, R.C., Lister, J.R., 1993. Dike transport of granitoid magmas. Geology 21 (9), 845–848.
Putirka, K.D., Canchola, J., Rash, J., Smith, O., Torrez, G., Paterson, S.R., Ducea, M.N., 2014. Pluton assembly and the genesis of granitic magmas: insights from the GIC pluton in cross section, Sierra Nevada Batholith, California. American Mineralogist 99 (7), 1284–1303.
Rodríguez, N., Díaz-Alvarado, J., Rodríguez, C., Riveros, K., Fuentes, P., 2016. Petrology, geochemistry and thermobarometry of the northern area of the Flamenco pluton, Coastal Range batholith, northern Chile. A thermal approach to the emplacement processes in the Jurassic Andean batholiths. Journal of South American Earth Sciences 67, 122–139.
Sawka, W., Chappell, B., Kistler, R., 1990. Granitoid compositional zoning by side-wall boundary layer differentiation: evidence from the Palisade Crest Intrusive Suite, central Sierra Nevada, California. Journal of Petrology 31 (3), 519–553.
Schoene, B., Schaltegger, U., Brack, P., Latkoczy, C., Stracke, A., Günther, D., 2012. Rates of magma differentiation and emplacement in a ballooning pluton recorded by U–Pb TIMS-TEA, Adamello batholith, Italy. Earth and Planetary Science Letters 355, 162–173.
Shellnutt, J.G., Bhat, G.M., Wang, K.-L., Brookfield, M.E., Dostal, J., Jahn, B.-M., 2012. Origin of the silicic volcanic rocks of the Early Permian Panjal Traps, Kashmir, India. Chemical Geology 334, 154–170.
Shirley, D.N., 1986. Compaction of igneous cumulates. The Journal of Geology 94 (6), 795–809.
Sisson, T., Bacon, C., 1999. Gas-driven filter pressing in magmas. Geology 27 (7), 613–616.
Sleep, N.H., 1974. Segregation of magma from a mostly crystalline mush. Geological Society of America Bulletin 85 (8), 1225–1232.
Sliwinski, J., Bachmann, O., Ellis, B., Dávila-Harris, P., Nelson, B., Dufek, J., 2015. Eruption of shallow crystal cumulates during explosive phonolitic eruptions on Tenerife, Canary Islands. Journal of Petrology, egv068.
Streck, M.J., 2014. Evaluation of crystal mush extraction models to explain crystal-poor rhyolites. Journal of Volcanology and Geothermal Research 284, 79–94.
Wall, R., Lara, L., Pérez de Arce, C., 2001. Upper Pliocene-Lower Pleistocene 40 Ar/39 Ar Ages of Pudahuel Ignimbrite (Diamante-Maipo Volcanic Complex), Central Chile (33.5 0 S).
Waples, D.W., Waples, J.S., 2004. A review and evaluation of specific heat capacities of rocks, minerals, and subsurface fluids. Part 1: minerals and nonporous rocks. Natural Resources Research 13 (2), 97–122.
Weinberg, R.F., 2006. Melt segregation structures in granitic plutons. Geology 34 (4), 305–308.
Zhang, J.-Y., Ma, C.-Q., Zhang, C., Li, J.-W., 2014. Fractional crystallization and magma mixing: evidence from porphyritic diorite-granodiorite dykes and mafic microgranular enclaves within the Zhoukoudian pluton, Beijing. Mineralogy and Petrology 108 (6), 777–800.